Investigation of the mechanism of upconversion luminescence in Er^{3+}/Yb^{3+} co-doped $Bi_2Ti_2O_7$ inverse opal

Dong Yan (严 冬), Zhengwen Yang (杨正文)*, Jiayan Liao (廖佳燕), Hangjun Wu (吴航俊), Jianbei Qiu (邱建备), Zhiguo Song (宋志国), Dacheng Zhou (周大成), Yong Yang (杨 勇), and Zhaoyi Ying (尹兆益)

Key Laboratory of Advanced Materials in Rare and Precious and Non-ferrous Metals, Ministry of Education, Key Laboratory of Advanced Materials of Yunnan Province, College of Materials Science and Engineering, Kunming University of Science and Technology, Kunming 650093, China

**Corresponding author: yangzw@kmust.edu.cn*

Received August 29, 2012; accepted January 25, 2013; posted online March 28, 2013

Three-dimensional-ordered Yb/Er co-doped $Bi_2Ti_2O_7$ inverse opal, powder, and disordered reference samples are prepared and their upconversion (UC) emission properties and mechanisms are investigated. Significant suppression of UC emission is detected when the photonic band-gaps overlap with Er^{3+} UC green emission bands. Interestingly, green and red UC emissions follow a two-photon process in the powder sample but a three-photon one in the inverse opal.

OCIS codes: 160.4760, 160.5298.
doi: 10.3788/COL201311.041602.

Photonic crystals are artificial periodic structures consisting of different dielectric materials in which the index of refraction varies in the visible wavelength scale[1,2]. The periodicity of photonic crystals leads to the formation of a photonic band-gap that can inhibit the propagation of light within a particular wavelength range that satisfies the Bragg condition. Therefore, spontaneous emission is modified if a material that ordinarily emits light is introduced into photonic crystals[1,3−6]. Controlling the spontaneous emission of materials is crucial for several practical applications, including low threshold lasers, high-efficiency light-emitting diodes, and even displays[7−10]. Therefore, when the controlling potential of spontaneous emission was proposed by the photonic crystals, several efforts were made to investigate modified spontaneous emissions in photonic crystals[3,4,11]. Earlier investigations focused on one-photon-excited down conversion luminescence, and few studies have reported the upconversion (UC) emission properties of photonic crystals[11−13]. Markowicz *et al.* found a sharp decrease in the UC emission of dyes within the band-gap range and a sharp enhancement at the band-gap edge[14]. Other studies reported that the UC emission lifetimes of $NaYF_4$:Yb,Er nanoparticles within photonic crystal structures may be altered[13]. In our previous study, we found that short wavelength UC emissions from the upper state are obviously enhanced due to inhibition of spontaneous UC emissions from the intermediate excited state in photonic crystals[15]. Despite these promising findings, however, few studies have investigated the mechanism of UC emission in photonic crystals. Understanding the mechanism of spontaneous UC emission from active materials embedded in a photonic crystal is fund a mentally important in the field of quantum optics and may bring about technological breakthroughs in UC devices, such as highly efficient solar cells and low-threshold lasers. Thus, we prepared three-dimensional-ordered Yb/Er co-doped $Bi_2Ti_2O_7$ inverse opal, powder, and disordered reference samples (RS) in this letter and investigated their UC emission properties and mechanisms.

The unitary ordered opal template grown from polystyrene microspheres of 400 diameter nm and the binary disordered template grown from mixed microspheres of 220- and 400-nm diameters were prepared by vertical deposition, as reported previously[11]. $Bi_2Ti_2O_7$ inverse opal photonic crystals were prepared using $Bi_2Ti_2O_7$:Yb,Er sol to infiltrate the opal template voids. Briefly, $Bi_2Ti_2O_7$:Yb (10% mol), Er (5% mol) sol was prepared using tetrabutyl titanate ($C_{16}H_{36}O_4Ti$), $Bi(NO_3)_3$, Yb_2O_3, and Er_2O_3 as raw materials. The rare earth nitrates were obtained by dissolving Yb_2O_3 and Er_2O_3 in hot nitric acid and subsequently evaporated. The rare earth nitrates and $Bi(NO_3)_3$ were dissolved in ethanol and glacial acetic acid, respectively, and then dropped into $C_{16}H_{36}O_4T$ lowly. The $Bi_2Ti_2O_7$:Er,Yb sol was obtained and used to infiltrate into the voids of the opal templates. $Bi_2Ti_2O_7$:Er,Yb inverse opal was obtained by sintering infiltrated sol templates at 670 °C for 5 h. $Bi_2Ti_2O_7$ inverse opal photonic crystals prepared from the ordered and disordered templates were denoted as IPC-I and the disordered RS, respectively. For comparison, a $Bi_2Ti_2O_7$:Er,Yb powder sample was prepared by sintering dyed $Bi_2Ti_2O_7$ gel.

Scanning electron microscopy (SEM, PHILIPS XL 30ESEM-TMP) was used to characterize and inspect the microstructure of the opal templates and inverse opal. The transmittance and UC emission spectra of the inverse opal were determined using a HITACHIU-4100 instrument and F-7000 spectrophotometer, respectively. X-ray diffraction (XRD) patterns of the inverse opal were recorded using a Rigaku 2 200 diffract ometer system.

A $Bi_2Ti_2O_7$:Er,Yb precursor solution is used to infiltrate into the voids of the opal templates, and the inverse opal is obtained by heat treatment. The XRD spectra of the inverse crystal are obtained to determine

its crystalline nature. Figure 1 shows the XRD pattern of the Er^{3+}/Yb^{3+} co-doped $Bi_2Ti_2O_7$ inverse opal photonic crystal. The spectrum indicate speaks at 14.862, 29.937, 34.796, 38.101, 49.968, and 59.655, respectively corresponding to reflections from the (222), (444), (800), (662), (880), and (1244) planes of $Bi_2Ti_2O_7$. This result confirms that the $Bi_2Ti_2O_7$ sol in the photonic crystal voids crystallizes after high-temperature treatment to yield cubic phase $Bi_2Ti_2O_7$[16–18].

The morphologies of the fabricated opal templates and inverse opals are observed by SEM to understand their lattice arrangement and surface quality. Self-assembly of single microspheres of 400-nm diameter into a face-centered cubic (fcc) lattice leads to the formation of an ordered opal, as shown in Fig. 2(a). This opal acts as a template for the preparation of three-dimensional-ordered inverse opal photonic crystals. Figure 2(d) shows an SEM image of IPC-I prepared from the ordered template. The inverted structure is well preserved by replicating opal voids with the resulting $Bi_2Ti_2O_7$ replica. The $Bi_2Ti_2O_7$ inverse opal exhibits a three-dimensionally-ordered structure comprising interconnected macropores that form an ordered hexagonal arrangement of air spheres. The template consisting of mixed microspheres of 220- and 400-nm diameters features a disordered structure, as shown in Fig. 2(b). Figure 2(c) shows an SEM image of the disordered RS. In this sample, randomly arranged air spheres may be observed.

Characterization of the optical transmittance of the photonic crystals can provide information about the position of the photonic band-gap. The optical transmittance spectra collected from IPC-I and RS when the incidence is vertical to the (111) plane are shown in Fig. 3. IPC-1 displays a deep photonic band-gap centered at 551 nm. By contrast, no photonic band-gap is found in the disordered RS.

Figure 4(a) shows the UC emission spectra of IPC-I and disordered RS. The UC spectra mainly consist of narrow emission lines corresponding to well-known Er^{3+} emissions from $^2H_{11/2}$,$^4S_{3/2}$ $\rightarrow$$^4I_{15/2}$ (524, 546, 556 nm) and $^4F_{9/2}\rightarrow$ $^4I_{15/2}$ (659 and 675 nm) transitions. The UC spectra in Fig. 4(a) are normalized to red emission to investigate the effect of the photonic stop band on UC emission. The intensity of green UC emission is significantly decreased in IPC-I compared with that in the disordered RS. The suppression of UC emission from the $Bi_2Ti_2O_7$:Yb,Er inverse opal near the

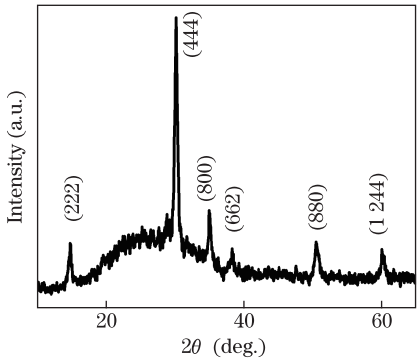

Fig. 1. XRD pattern of the $Bi_2Ti_2O_7$ inverse opal.

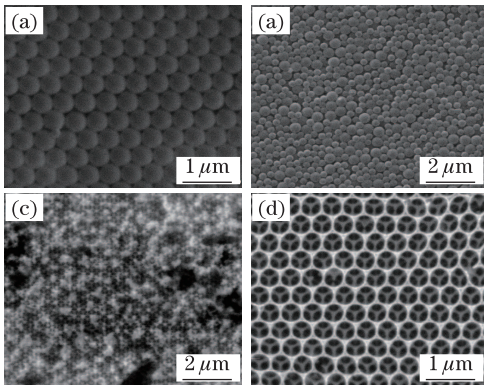

Fig. 2. SEM images of (a) direct and (d) inverse opals made of polystyrene microspheres (diameter, 400 nm). SEM images of (b) direct and (c) reference sample constructed with polystyrene microspheres (diameters, 400 and 220 nm).

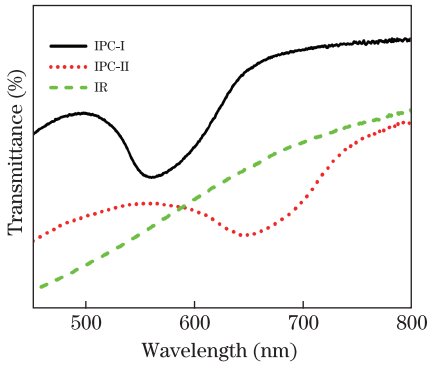

Fig. 3. Transmittance spectra of IPC-I and the reference sample.

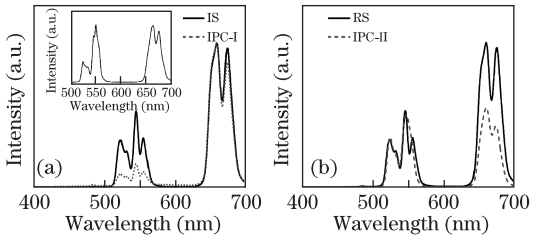

Fig. 4. Upconversion emission spectra of (a) IPC-I and the reference sample and (b) IPC-II and the reference sample.

center of the photonic band-gap may be attributed to the inhibition of spontaneous emission by the photonic band-gap. We prepared another type of inverse opal (denoted as IPC-II) with a photonic band-gap located at 656 nm (Fig. 3) and studied its optical UC properties to confirm whether or not the suppression of UC emission is caused by the presence of the photonic band-gap. The UC emission spectra of IPC-II and the disordered RS are shown in Fig. 4(b). The intensity of red UC emission of IPC-II is lower than that of the disordered RS, thereby confirming that the suppression of UC emission in the $Bi_2Ti_2O_7$: Yb,Er inverse opal near the center of the photonic band-gap results from photonic band-gap effects.

The photon numbers involved in the green and red UC emission processes were investigated by analyzing the dependence of UC emission intensity on the excitation power. Figures 5(a)–(c) show the behaviors of the green and red UC emissions as a function of the excitation

power in the disordered RS, IPC-I, and powder sample, respectively. Red and green UC emissions exhibit a linear dependence on the excitation power in IPC-I, the powder sample, and the disordered RS. In the powder sample, the slopes of the $^2H_{11/2}\rightarrow{}^4I_{15/2}$ (524 nm), $^4S_{3/2}\rightarrow{}^4I_{15/2}$ (546 and 556 nm), and $^4F_{9/2}\rightarrow{}^4I_{15/2}$ (659 and 675 nm) transitions of Er^{3+} are close to 2, indicating that a two-photon process is involved in the green UC emission. The n values for green and red UC emissions are much larger than 2 in IPC-I and the disordered RS, indicating a three-photon process. The two-photon process for green and red UC emissions of Er^{3+} has been extensively reported in Er^{3+} doped materials under 980-nm excitation[19,20]. Interestingly, green and red UC emissions of the powder sample follow a two-photon process whereas those of the $Bi_2Ti_2O_7$:Yb, Er inverse opal follow a three-photon one under 980-nm excitation.

The mechanism of UC emission was investigated based on the energy level diagram of Er^{3+} and Yb^{3+}. Figure 6 shows a typical energy-level diagram for UC emissions under 980-nm excitation. For the two-photon process of the powder sample, Er^{3+} ions are excited to the $^4I_{11/2}$ state from the $^4I_{15/2}$ ground state by direct excitation or energy transfer (ET) from the Yb^{3+} excited directly by incident light. Electrons in $^4I_{11/2}$ can be further excited to the $^4F_{7/2}$ state by excited-state absorption (ESA) and/or ET. Electrons in $^4F_{7/2}$ relax to the $^2H_{11/2}$ and $^4S_{3/2}$ states. Radiative transitions from the $^2H_{11/2}$ and $^4S_{3/2}$ states to $^4I_{15/2}$ could result in green UC emissions[20]. Electrons in the $^4I_{11/2}$ excited state may also relax to the low-lying $^4I_{13/2}$ level. Electrons in the $^4I_{13/2}$ excited state can absorb energy from 980-nm excitation light or a second ET from a neighboring Yb^{3+}ion, leading to further excitation from $^4I_{13/2}$to $^4F_{9/2}$. Finally, radiative transitions from the $^4F_{9/2}$ to $^4I_{15/2}$ states take place, resulting in red emissions at 659 and 675 nm.

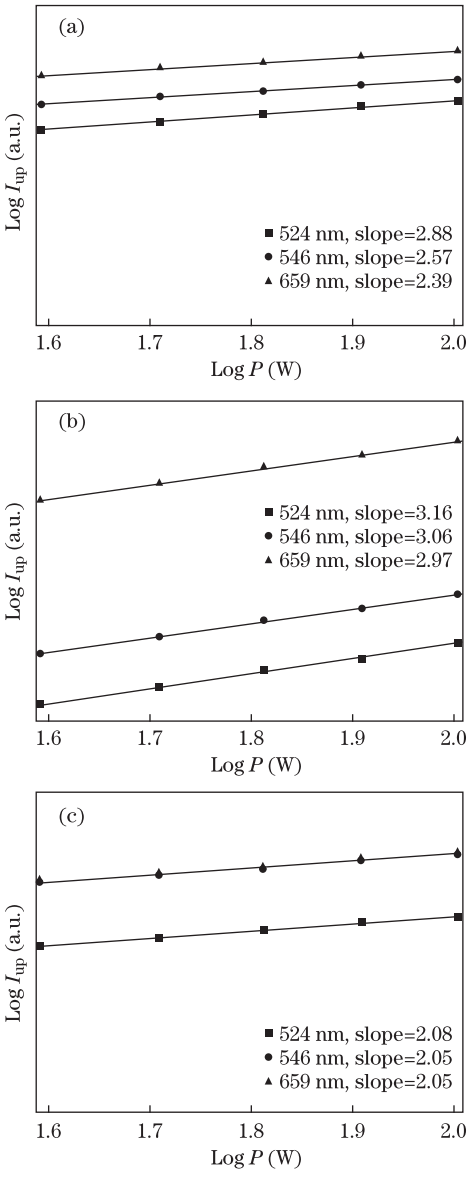

Fig. 5. Power dependence of the upconversion emission intensities of (a) the disordered reference sample, (b) IPC-I, and (c) the powder sample under 980-nm laser excitation.

For IPC-I and the disordered RS, UC emissions appear to follow the three-photon process. Electrons in the $^4F_{9/2}$ excited state can be further excited to the $^4G_{11/2}$ level by a third ET and/or ESA. Electrons in the $^4G_{11/2}$ excited state can also relax rapidly and non-radiatively to the $^2H_{11/2}$ and $^4S_{3/2}$ levels, leading to green UC emissions. During green UC emission from the three-photon process, the number of electrons in green emission states ($^2H_{11/2}$ and $^4S_{3/2}$) is related to the $^4F_{9/2}$ state. Therefore, a large number of electrons in the $^4F_{9/2}$ level is favorable for the three-photon process. The powder sample and IPC-I/disordered RS demonstrate two-and three-photon processes of green UC emission, respectively, due to differences in the populations of their $^4F_{9/2}$ levels. Figure 7 shows the FT-IR spectra of IPC-I, the disordered RS, and the powder sample. The 1 650 and 3 460 cm^{-1} bands contribute to the vibration of the OH^- groups. The energy gap between the $^4I_{11/2}$ and $^4I_{13/2}$ states is about 3 600 cm^{-1}, matching the hydroxyl phonon energy ($\sim$3 460 cm^{-1}) well. Non-radiative relaxation from $^4I_{11/2}$ to $^4I_{13/2}$ can be significantly enhanced through cross ET to the OH^- group, resulting in an increase in the number of electrons in the $^4I_{13/2}$ state. The number of electrons in the $^4F_{9/2}$ level is proportional to that in the $^4I_{13/2}$ state, as shown in Fig. 6. The FT-IR spectra indicate that the intensity of the OH^- group of the powder sample is weaker than those of IPC-I and the disordered RS because the relatively larger surface areas of the lateral low a larger number of OH^- groups to attach to their surfaces. Therefore, increasing the non-radiative relaxation rate from $^4I_{11/2}$ to $^4I_{13/2}$ states by cross ET to the OH^- group can enhance the number of electrons in the $^4I_{13/2}$ and $^4F_{9/2}$ states in IPC-I and the disordered RS, leading to the green UC emission of the three-photon process. The energy gap (3 700 cm^{-1}) between the $^4S_{3/2}$ and $^4F_{9/2}$ states matches the hydroxyl phonon energy ($\sim$3 460 cm^{-1}) and may increase non-radiative relaxation from the $^4S_{3/2}$ to $^4F_{9/2}$ states to the OH^- group through cross ET. More OH^- groups are favorable for enhancing the three-photon process of red UC emission, and the n value in the disordered RS thus increases to 2.39

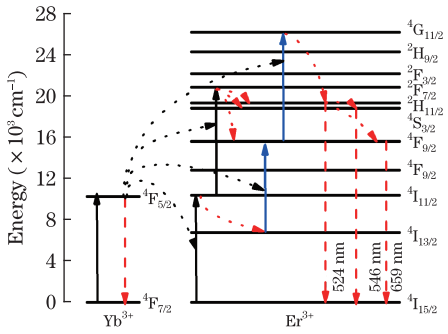

Fig. 6. Energy level diagrams of Yb^{3+} and Er^{3+} ions and the proposed upconversion emission mechanism.

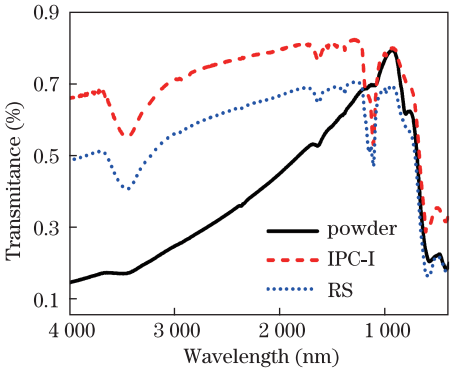

Fig. 7. FT-IR spectra of IPC-I, the disordered reference sample, and the powder sample.

compared with the powder sample. Electrons in the $^2H_{11/2}$ and $^4S_{3/2}$ excited states can relax non-radiatively to the $^4F_{9/2}$ level or transit to the $^4I_{15/2}$ ground state through spontaneous emission, as shown in Fig. 6. Suppression of spontaneous emissions from the $^2H_{11/2}$ and $^4S_{3/2}$ levels to $^4I_{15/2}$ in the photonic crystal enhances non-radiative decay from $^2H_{11/2}$ and $^4S_{3/2}$ to $^4F_{9/2}$. Thus, red UC emission of the three-photon process may be observed in the $Bi_2Ti_2O_7$:Yb,Er inverse opal. Other experimental results, such as lifetime measurements, may be helpful in further elucidating the mechanism of UC emission. As such, further investigations on the $Bi_2Ti_2O_7$:Yb,Er inverse opal are necessary.

In conclusion, three-dimensionally-ordered macroporous $Bi_2Ti_2O_7$: Yb, Er inverse opal photonic crystals are successfully fabricated using polystyrene colloidal crystals as a template and the mechanism of their UC emission is investigated. Under 980-nm excitation, green (Er^{3+}: ($^2H_{11/2}$, $^4S_{3/2}$) $\rightarrow$$^4I_{15/2}$) UC emission is significantly suppressed. The mechanism of UC emission of Er^{3+} is also discussed. Green and red UC emissions of the three-photon process are observed in the inverse opal.

This work was supported by the Natural Science Foundation of Yunnan Province (No. 2010ZC038), the Open Foundation of Key Laboratory of Advanced Materials in Rare, Precious and Non-ferrous Metals, Ministry of Education, and the Open Foundation of Key Laboratory of Advanced Materials of Yunnan Province (No. ZDS2010011B).

References

1. E. Yablonovitch, Phys. Rev. Lett. **58,** 2059 (1987).
2. S. John, Phys. Rev. Lett. **58,** 2486 (1987).
3. Z. Yang, X. Huang, L. Sun, J. Zhou, B. Li, and C. Yu, J. Am. Ceram. Soc. **92,** 1596 (2009).
4. Z. Yang, J. Zhou, X. Huang, G. Yang, Q. Xie, and L. Sun, Chem. Phys. Lett. **445,** 55 (2008).
5. R. F. Nabiev, P. Yeh, and J. J. Sanchez-Mondragon, Phys. Rev. A **47,** 3380 (1993).
6. S. John and T. Quang, Phys. Rev. A **50,** 1764 (1994).
7. K. Ziemelis, Nature **399,** 408 (1999).
8. M. Loncar, T. Yoshie, A. Scherer, P. Gogna, and Y. M. Qiu, Appl. Phys. Lett. **81,** 2680 (2002).
9. H. Ichikawa and T. Baba, Appl. Phys. Lett. **84,** 457 (2004).
10. C. E. Finlayson, D. S. Ginger, and N. C. Greenham, Chem. Phys. Lett. **338,** 83 (2001).
11. Z. Yang, D. Yan, K. Zhu, Z. Song, X. Yu, D. Zhou, Z. Yin, and J. Qiu, Mater. Lett. **65,** 1245 (2011).
12. Z. Li, L. Li, H. Zhou, Q. Yuan, C. Chen, L. Sun, and C. Yan, Chem. Commun. **43,** 6616 (2009).
13. F. Zhang, Y. Deng, Y. Shi, R. Zhang, and D. Zhao, J. Mater. Chem. **20,** 3895 (2010).
14. P. Markowicz, C. Friend, Y. Shen, S. Jacek, and N. P. Paras, Opt. Lett. **27,** 351 (2002).
15. Z. Yang, D. Yan, K. Zhu, Z. Song, X. Yu, D. Zhou, Z. Yin, and J. Qiu, Mater. Chem. Phys. **133,** 584 (2012).
16. S. Y. Chen, C. C. Ting, and W. F. Hsieh, Thin Solid Films **434,** 171 (2003).
17. W. Wang, Q. Shang, W. Zheng, H. Yu, X. Feng, Z. Wang, Y. Zhang, and G. Li, J. Phys. Chem. C **114,** 13663 (2010).
18. C. P. Sibu, S. R. Kumar, P. Mukundan, and K. G. K. Warrier, Chem. Mater. **14,** 2876 (2002).
19. X. Qu, H. Song, X. Bai, G. Pan, B. Dong, H. Zhao, F. Wang, and R. Qin, Inorganic Chemistry **47,** 9654 (2008).
20. H. Song, B. Sun, T. Wang, S. Lu, L. Yang, B. Chen, X. Wang, and X. Kong, Solid State Commun. **132,** 409 (2004).